ASME Journal of Tribology
Online journal at:
https://asmedigitalcollection.asme.org/tribology

Mohamed Kalifa[1]
Centre for Life-Cycle Engineering and Management,
Faculty of Engineering and Applied Sciences,
Cranfield University,
Cranfield MK43 0AL, UK
e-mail: mohamed.kalifa@cranfield.ac.uk

Muhammad Khan
Centre for Life-Cycle Engineering and Management,
Faculty of Engineering and Applied Sciences,
Cranfield University,
Cranfield MK43 0AL, UK
e-mail: muhammad.a.khan@cranfield.ac.uk

Feiyang He
Centre for Life-Cycle Engineering and Management,
Faculty of Engineering and Applied Sciences,
Cranfield University,
Cranfield MK43 0AL, UK
e-mail: feiyang.he@cranfield.ac.uk

Kanza Basit
Department of Engineering Sciences,
National University of Sciences and Technology (NUST),
Sector H-12,
Islamabad 44000, Pakistan
e-mail: kanza.basit@pnec.nust.edu.pk

Hilal Doganay Kati
Centre for Life-Cycle Engineering and Management,
Faculty of Engineering and Applied Sciences,
Cranfield University,
Cranfield MK43 0AL, UK;
Faculty of Engineering and Natural Sciences,
Department of Mechanical Engineering,
Bursa Technical University,
16310 Bursa, Turkey
e-mails: Hilal.Doganay@cranfield.ac.uk

Analytical Modeling and Experimental Validation of Wear and Frictional Noise Under Lubricated Conditions

Understanding the dynamics of friction, wear, and noise under lubricated conditions is crucial for the predictive maintenance of mechanical systems; however, existing models often overlook the role of lubrication in modulating these interactions. This research presents an analytical model that combines single-degree-of-freedom (SDOF) vibration theory, Hertz contact mechanics, the Archard wear model, and the principles governing acoustic emission to predict both wear depth and sound pressure level emitted in a lubricated pin-on-disc system. Contact stiffness and wear-induced geometric changes are dynamically updated by the model, considering viscous damping from thin-film lubrication. Experiments were conducted using an Anton Paar TRB3 tribometer under lubricated conditions at realistic loads of 15, 20, and 30 N and a rotational speed of 300 rpm (corresponding to a linear sliding velocity of approximately 0.314 m/s at a 10-mm track radius). The friction noise was recorded by a microphone that was free-standing. The analytical predictions were closely aligned with the measurements taken during the tests. For mild steel, wear depth errors remained below 22%, while sound pressure predictions deviated by 14–21%. Due to its softer nature, aluminum exhibited higher wear deviations (up to 32%). Track analyses showed that lubrication decreases wear depth compared to dry sliding, and sound pressure levels are closely related to wear depth. Track analysis revealed that lubrication decreases wear depth by up to 50% compared to dry sliding, and sound pressure levels closely follow wear progression. This work improves prognostic health management systems by incorporating lubrication dynamics and tribo-acoustic phenomena, which allow for effective real-time wear and noise monitoring in industrial applications.
[DOI: 10.1115/1.4069335]

Keywords: friction, wear, wear modeling, lubrication, fluid film lubrication, single-degree-of-freedom (SDOF), Hertzian contact mechanics, pin-on-disc systems, frictional noise, tribological conditions, surface hardness, surface roughness and asperities, acoustic emission

1 Introduction

To improve the operational efficiency and durability of mechanical systems, it is essential to understand the complex interconnections between friction, wear, acoustic emissions, and lubrication; for example, friction causes wear, and both can create noise. Lubrication plays a key role by reducing contact between surfaces, reducing wear, decreasing system vibrations, and lowering noise emissions. Industrial applications and research become more important as demands for higher performance and longer service life increase [1–3]. Real-time monitoring of these tribological processes is still a challenge. Despite being widely used for machine health monitoring, vibration-based sensing can be insufficiently sensitive or impractical in certain operational environments. High-frequency stress waves emitted by microscopic events at contact interfaces have become a focus of acoustic monitoring. These acoustic emissions (AE), along with other terms and symbols used throughout the study, are defined in the Nomenclature and are indicative of frictional behavior, surface wear, and lubrication breakdown [4–9].

[1]Corresponding author.

Contributed by the Tribology Division of ASME for publication in the Journal of Tribology. Manuscript received April 16, 2025; final manuscript received July 30, 2025; published online August 26, 2025. Assoc. Editor: Athanasios Chasalevris.

Despite the clear advantages of AE-based methods, most existing analytical and numerical models still address friction and wear separately, rarely incorporating acoustic emissions and lubrication effects into a unified predictive model [10–13]. AE signals are sensitive to frictional behavior, lubrication regimes, and wear mechanisms, enabling real-time anomaly detection, wear estimation, and failure prediction [14–17]. Pioneering studies by Akay [18] attributed friction-induced noise under high pressures to mechanical instabilities at asperity junctions, while Stoimenov et al. [19] and Ben Abdelounis et al. [20] linked spectral noise changes to surface roughness. Yokoi and Nakai [21] further correlated elevated noise levels with increased coefficient of friction. Recent advances by Wang et al. [22] and Towsyfyan et al. [23] have demonstrated the advantages of AE in evaluating tribological performance. Othman and Elkholy [24] and Shahid et al. [25] have validated acoustic techniques for quantifying surface roughness and predicting wear.

The integration of machine learning and signal processing in emerging methodologies is now possible to enhance predictive accuracy. Chen et al. [26] employed neural networks to determine wear states from polymer friction noise, achieving real-time precision. Wang [27] generalized wear–noise relationships across materials via transfer learning. Raja et al. [28] applied Hilbert transform-based envelope analysis to identify wear levels from acoustic signatures. However, challenges persist under lubricated conditions. Khan et al. [29] reported inconsistencies in airborne noise due to lubrication variability, and Tian et al. [30] and Lontin et al. [31] highlighted temperature-dependent effects on wear distribution and acoustic emissions. The intricate interrelationship between friction, wear, lubrication, and acoustic emissions is highlighted in these investigations, but a coherent analytical model is still not achievable. The use of acoustic emission signals in prognostic health management systems is increasing, indicating stress waves that are caused by the deformation and fracturing of materials during frictional sliding [32–37]. While vibration-based models detect advanced-stage wear [38–40], frictional noise can offer an early warning of surface interaction conditions [5,41,42].

Le Bot [43] investigated the origin of friction noise on rough surfaces and found that it is caused by collisions between surface asperities. An adhesive and abrasive wear in metal systems was traced by Seong et al. [44] using acoustic signals, Haar wavelet coefficients, and peak signal-to-noise ratio. Wavelet analysis was able to differentiate between these wear types by examining changes in contact pressure. Although this approach appears promising for real-time wear monitoring, it relies on a specific setup and requires further development for more complex conditions. Albuquerque de Freitas et al. [45] employed finite element simulations to investigate the impact of factors such as brake pressure and friction coefficient on friction wear and brake squeal. Ma et al. [46] investigated the influence of circular pits, introduced into the surface of a friction brake, on the generation of squeal noise during dry sliding, revealing that the incorporation of such textures has the potential to postpone the emission of high-intensity frictional noise. This demonstrates the significance of surface texture in reducing friction noise and wear in dry contact mechanisms. Similarly, Zhang et al. [47] explored the implications of grooved textures in lubrication scenarios involving sand-containing oils, illustrating that the grooves effectively captured particulate matter, mitigated surface abrasions, and enhanced wear resistance. The vibration and noise levels of tapered roller bearings with textured surfaces were significantly lower than those with smooth surfaces when they were not lubricated [48]. Furthermore, Liu et al. [49] examined different surface textures on stainless-steel specimens. Their observation that noise levels could be reduced by up to 66% reinforces the significance of surface texturing in reducing friction-induced noise.

Acoustic emissions have been explored by many researchers in tribological studies, in addition to airborne noise. Boness and McBride, for example, investigated how acoustic emissions evolve throughout the wear process [50–52], and an experiment examined the effect of lubrication on these emissions, finding a good correlation between wear rate and acoustic emission [5]. At the same time, Benabdallah and Aguilar [53] focused their research on how AE signals can predict airborne noise levels. The close relationship between wear, lubrication, and acoustic emission is highlighted by these studies. Despite these advances, there is still a significant gap in the literature regarding comprehensive analytical models that incorporate AE with both wear phenomena and airborne noise. In the domain of friction modeling, De Moerlooze et al. [54] introduced a theoretical model predicated on asperity contact mechanics for the analysis of friction; however, it failed to account for wear phenomena. Eriten et al. [55] and Emami et al. [56] have demonstrated more advanced friction models based on asperity interactions, but they did not consider wear mechanisms. Despite the existence of numerous numerical models designed for elastoplastic contact interfaces [57], they fail to consider sound generation. This creates a significant gap: there is no unified framework that links wear processes, friction behavior, and both AE and airborne noise in a predictive manner under lubricated conditions.

According to the literature reviewed, at least three different analytical models have attempted to link friction, wear, and noise, but with limited scope or accuracy. Tian et al. [58] introduced empirical-analytical equations related to Ball-on-Disc friction, wear, and noise, specifically formulated for an aluminum-based model. This model, which was derived from tribometer experimentation, establishes a quantitative correlation between wear volume, coefficient of friction, and sound pressure. Predictive equations are validated for aluminum, brass, and steel in specific load and speed ranges. Lontin and Khan [59] introduced an analytical approach to asperitical levels. The relationship between wear and airborne noise is calculated by this model using asperity contact mechanisms in dry conditions. An analytical analysis is used to estimate wear and sound pressure output. Basit et al. [60] presented a model that uses analytical vibration to estimate wear-sound. Vibrational responses are employed by this analytical model to determine incremental wear and characterize the associated acoustic emissions. The parameters of wear depth and frictional acoustics are quantitatively assessed and compared with experimental findings derived from pin-on-disc tests also conducted under dry conditions, yielding good agreement for both wear depth and sound pressure levels, as shown in Fig. 1.

In contrast to models developed under dry conditions, the present study proposes a new analytical model that incorporates lubrication as a key element that affects the friction, wear, and noise relationship. The aim is to address the wear depth and emitted sound pressure, which have been experimentally validated using a tribometer tester. The friction, wear, and noise relationships are integrated through this innovative analytical model that synthesizes single-degree-of-freedom (SDOF) vibration theory, Hertz contact mechanics, Archard's wear model, and principles of acoustic emission. Unlike Basit et al.'s dry-condition model, this work accounts for viscous damping from thin-film lubrication, which alters vibrational modes, wear rates, and acoustic emissions. Real-time predictions of emitted sound pressure levels under lubricated sliding conditions are possible due to the dynamic update of contact stiffness and wear depth by the model. This work introduces the first unified model integrating thin-film damping, dynamic stiffness updates, and acoustic emissions for lubricated systems, addressing a critical gap in tribo-acoustic prognostics.

2 Analytical Model Under Lubrication Conditions

The SDOF vibration theory, Hertz contact mechanics, Archard's wear model, and acoustic emission theory are combined in this work to examine the dynamic behavior of a pin–disc system. In this setup, a pin slides against a rotating disc with lubrication acting primarily as a damping mechanism, as illustrated schematically in Fig. 2. The model captures how wear modifies the overall stiffness, examines the corresponding vibrational response, and predicts the resulting acoustic emissions. In the context of the SDOF,

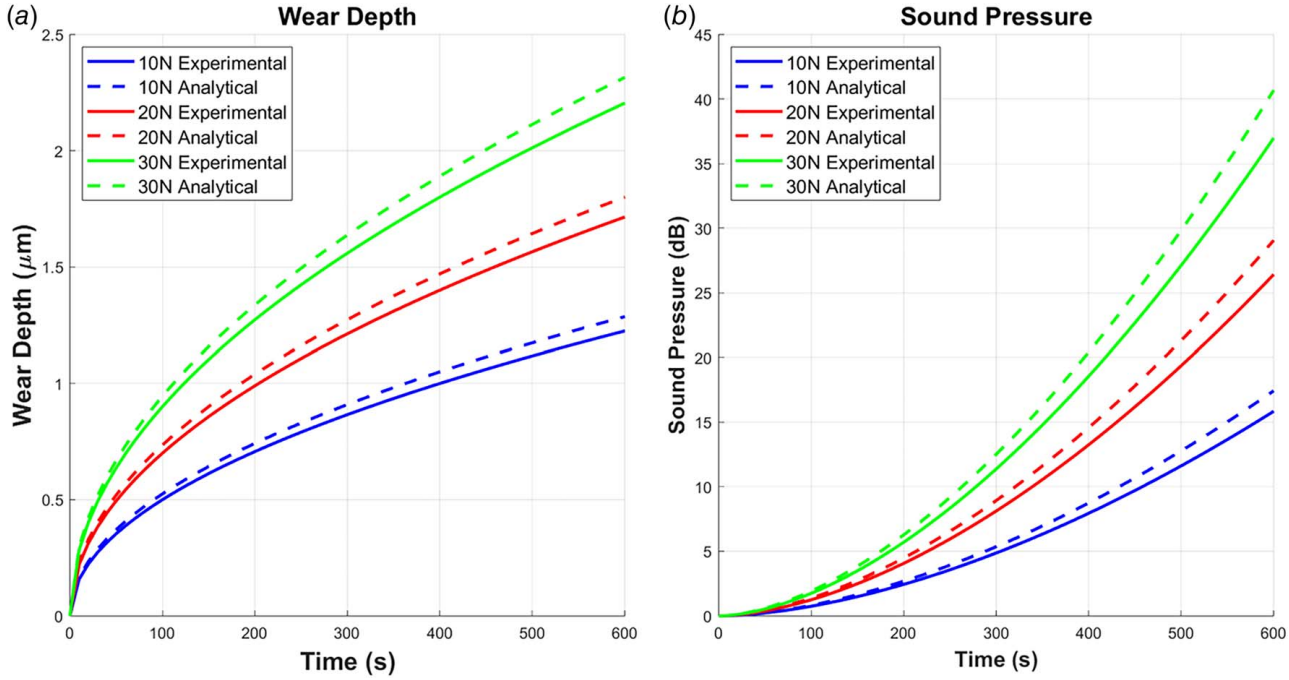

Fig. 1 Wear depth (*a*) and emitted sound pressure and (*b*) under dry-condition tests [60]

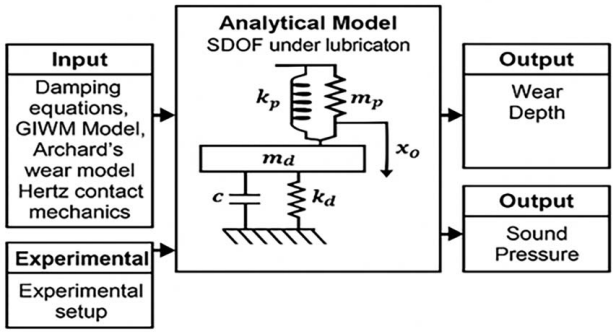

Fig. 2 Block diagram of the SDOF analytical model under lubrication

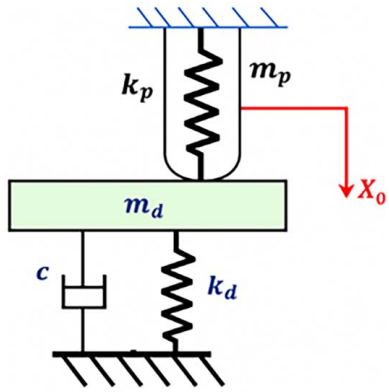

Fig. 3 Analytical model of SDOF

the pin is conceptualized as a mass-spring-damper system characterized by mass $\boldsymbol{m}$, stiffness $\boldsymbol{k}$, and the damping coefficient $\boldsymbol{c}$, as illustrated in Fig. 3. The disc contributes torsional stiffness k_t, while the lubricating layer provides additional viscous damping k. The Hertzian contact theory elucidates the normal contact stress and elastic deformation that occur between a spherical pin and a flat disc. At the same time, Archard's wear model quantifies the wear volume losses based on the applied load, sliding distance, material hardness, and the wear coefficient. Both the contact area and the effective stiffness are dynamically updated by these computations. Acoustic emission analysis then uses the pin's vibrational velocity to estimate acoustic power, converting it into sound pressure levels.

2.1 The Model is Subject to the Following Key Assumptions

- The pin is assumed to travel straight downward, with no sideways or rotational movement.
- Pin wear is considered negligible, reflecting the standard practice in pin-on-disc tribology, where the disc sustains the majority of the material losses.
- Surface roughness is ignored, ensuring that the Hertzian assumption of idealized geometry (spherical pin and flat disc) remains valid.
- Thin-film lubrication: The regime is boundary/mixed, so viscous damping dominates over hydrodynamic effects.
- Temperature and pressure do not affect the viscosity and damping coefficients of the lubricant.
- Frictional heating is negligible; therefore, temperature does not influence stiffness, damping, or wear rates.
- Sound pressure levels are calculated with the assumption of free-field radiation, without any reflections or impedance mismatches.

2.2 Equations of Motion and Solutions. The lubricated pin–disc apparatus is conceptualized as an SDOF underdamped oscillator, which is governed by the second-order linear differential equation, as given in the following equation [61,62]:

$$m\ddot{x} + c\dot{x} + k_{eq}x = F_n(\sin\bar{\omega}t) \tag{1}$$

where x is the displacement of the pin, $\dot{x}$ is the velocity, $\ddot{x}$ is the acceleration, k_{eq} is the equivalent stiffness of the system, and

$F_n \times \sin(\omega t)$ represents the external periodic force acting on the system.

The solution $x(t)$ describes the pin displacement over time, representing the wear losses of the disc, and is given by the following equation [62]:

$$x(t) = e^{-\zeta\omega_n t}(\, C_1 \cos\, \omega_d t \; + C_2 \sin\omega_d t) + \frac{\frac{F_0}{K}\sin(\bar{\omega}t - \phi)}{\sqrt{(1-r^2)^2 + (2r\zeta^2)^2}} \tag{2}$$

where C_1 and C_2 represent constants ascertained by the initial conditions, ζ is the coefficient of damping, ω_n is the inherent frequency, ω_d is the frequency observed with damping effects, and $\bar{\omega}$ is the forced frequency. The phase lag ϕ and the frequency ratio of the steady-state solution are given by the following equations:

$$\phi = \tan^{-1}\left(\frac{2r\zeta}{1-r^2}\right) \tag{3}$$

$$r = \frac{\varpi}{\omega} \tag{4}$$

The frequency of damped oscillations is determined by the following equation:

$$\omega_d = \omega_n \sqrt{1-\zeta^2} \tag{5}$$

The damping ratio can be calculated by the following equation:

$$\zeta = \frac{c}{c_c} \tag{6}$$

where c is the damping constant, which can be calculated by Eq. (7), and c_c is the critical damping coefficient and calculated by using Eq. (8):

$$c = \frac{F_F}{v_c} \tag{7}$$

where F_F is the frictional force and v is the velocity, which is calculated by $v_c = r_d \times \omega_n$, where r_d is the radius of the rotating disc:

$$c_c = 2m_p\omega_n \tag{8}$$

where m_p is the mass of the pin.

The natural frequency can be calculated by the following equation:

$$\omega_n = \sqrt{\frac{k_{\text{eq}}}{m_p}} \tag{9}$$

2.3 Stiffness of the Pin–Disc System. This section details the derivation of the equivalent stiffness k_{eq} for the lubricated pin disc system, incorporating torsional disc stiffness k_{tn}, axial pin stiffness k_p, and wear-induced geometric changes.

The torsional stiffness of the rotating disc is derived from classical elasticity theory and is given by the following equation [63]:

$$k_{tn} = \frac{GJ}{L_n} \tag{10}$$

where L_n the adequate contact depth is defined as being initially equivalent to the diameter of the pin (assumed to be spherical), G represents the rigidity modulus (shear modulus) of the disc material, and J denotes the polar moment of inertia, which the following equation computes.

$$J = \frac{\pi\, d^4}{32} \tag{11}$$

As the process of wear advances, the depth of contact L_n experiences an augmentation, subsequently leading to a decrease k_{tn}. Incorporating incremental wear depth h_{i+1} can be rewritten to account for incremental wear, as in the following equation:

$$k_{tn} = \frac{(\pi G D^4)}{32h_{i+1}} \tag{12}$$

where h_{i+1} represents the incremental wear depth, which influences the effective contact length L_n.

The pin stiffness of the pin k_p behaves like a linear compression spring, contributing to the overall stiffness, as shown in the following equation:

$$k_p = \frac{E_p A}{L} \tag{13}$$

where A denotes the surface area of the pin in contact with the disc, E_p represents the Young's modulus associated with the pin material, and L indicates the length of the pin.

The total equivalent stiffness of the system is obtained by combining the pin stiffness k_p and the disc torsional stiffness k_{tn}, expressed as in the following equation:

$$\frac{1}{k_{eq}} = \frac{1}{k_p} + \frac{1}{k_{tn}} \tag{14}$$

The collective rigidity of the system has a direct influence on the vibrational behavior of the pin–disc configuration. As wear progresses, effective contact length L_n changes, leading to variations in k_{eq}. This in turn modifies the total stiffness, causing shifts in the natural frequency ω_n of the system and damped natural frequency, which influences vibration behavior and sound generation.

2.4 Wear and Contact Mechanics. Archard's model establishes a foundational correlation for wear volume (V) contingent upon factors such as load (F_n), sliding distance (s), hardness (H), and a wear coefficient (k), which can be computed utilizing the following equation [64]:

$$V = \frac{ksF_n}{H} \tag{15}$$

In the context of a Hertzian contact [65], the contact radius, denoted as a, in conjunction with an effective radius R, is articulated through the expression delineated in the following equation:

$$a = \sqrt[3]{\frac{3F_N R}{4E}} \tag{16}$$

where F_N is the normal force.

For a spherical pin radius R_p against a disc radius R_d, the effective radius R can be calculated by the following equation:

$$\frac{1}{R} = \frac{1}{R_p} + \frac{1}{R_d} \tag{17}$$

The effective Young's modulus E can be calculated in the following equation:

$$\frac{1}{E} = \frac{1}{2}\left(\frac{1-\vartheta_p^2}{E_p} + \frac{1-\vartheta_d^2}{E_d}\right) \tag{18}$$

where the symbols denote Young's modulus associated with the pin E_p and disc E_d, respectively, while the other symbols signify Poisson's ratio, the pin ϑ_p and disc ϑ_d, respectively.

To determine the wear depth as a function of the sliding distance, the global incremental wear model is employed [66]. This theoretical model asserts the progression of the contact area within the geometry of an elliptical wear track. As illustrated in Fig. 4, the contact area is circular; however, as the sliding action advances, the wear track expands in the direction of motion, turning into an

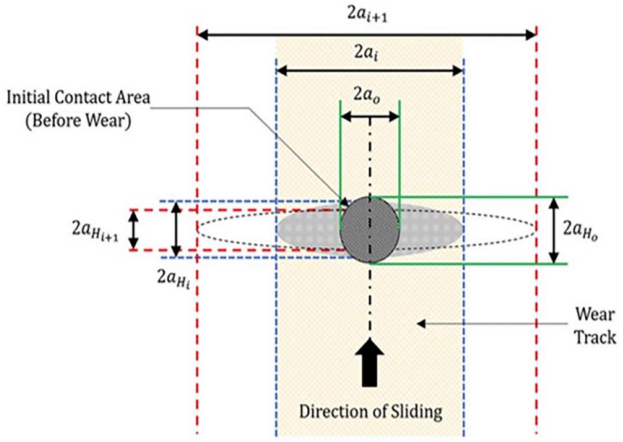

Fig. 4 The progression of the wear track manifests in an elliptical configuration [60]

ellipse. The minor axis (contact length 2aH) decreases while the major axis (wear track width, 2a) expands, culminating in an augmented contact area and consequently mitigating the contact pressure during subsequent sliding. The initial elastic deformation h_0^e can subsequently be assessed using the following equation:

$$h_0^e = \frac{F_n}{2Ea_0} \tag{19}$$

where h_0^e is the initial elastic deformation and a_0 is defined as the initial contact radius under circular contact.

Hertzian contact theory is used to determine the initial contact radius, which is assumed to be circular. As the wear process progresses, iterative calculations are carried out to assess the incremental changes in geometry and pressure related to each cycle until the maximum sliding distance is achieved. The incremental wear depth is measured as described in the following equation:

$$h_{i+1}^w = h_i^w + 2k_D p_i a_{Hi} \tag{20}$$

where h_{i+1}^w denotes the incremental wear depth at the position "$i+1$" concerning the sliding distance and h_i^w represents the wear depth at the position "i" relating to the sliding distance. k_D indicates the stiffness of the disc, and the average contact pressure, p_i n, can be determined through the application of the following equation:

$$p_i = \frac{F_N}{\pi a_{i+1} a_{Hi}} \tag{21}$$

The evaluation of elastic deformation occurring in a direction orthogonal to the contact surface may be performed using the well-documented Oliver and Pharr correlation, as described in the following equation:

$$h_{i+1}^e = \frac{F_N}{2E\sqrt{a_{i+1}a_{Hi}}} \tag{22}$$

To account for the transition from Hertz's rectangular contact area assumption to the elliptical model, a correction factor π is introduced. The lesser axis of the contact ellipse a_{Hi} is articulated in the following equation:

$$a_{Hi} = 2\sqrt{\frac{F_n R}{\pi a_{i+1}\pi E}} \tag{23}$$

As a result, the total wear depth h_{i+1} is accordingly represented as a function of initial elastic deformation h_{i+1}^w and incremental wear depth, as calculated by the following equation:

$$h_{i+1} = h_i^e + h_{i+1}^w \tag{24}$$

By implementing a substitution h_{i+1} for the cumulative wear depth as articulated in Eq. (12), the temporal variation of the disc's stiffness (specifically, the torsional stiffness) provides more understanding and can be calculated by the following equation:

$$k_t = \frac{\pi G D^4}{32 h_{i+1}(h_i^e + h_{i+1}^w)} \tag{25}$$

The natural frequency of the mechanical system, primarily governed by the stiffness properties of the disc and pin, can now be thoroughly assessed by assigning a theoretically justified preliminary mass. Furthermore, the wear coefficient—an essential factor in the system's dynamics—is variable and can change significantly due to fluctuations in volume loss during operation. The results obtained from the use of these mathematical equations are systematically reintegrated into Eq. (1) to gain a better understanding of the system's behavior over the specified duration. It is necessary to accurately determine the pin's displacement as a function of time. The initial displacement x_0 of the system can be calculated by using Eq. (26), which serves as a crucial tool for quantifying the initial conditions of the mechanical system under analysis.

2.5 Vibration Response to Calculate Wear Rate. x_0 is the initial displacement, which is assumed to be the elastic displacement, and it can be defined from the following equation:

$$x_0 = \frac{F_N}{2Ea} \tag{26}$$

Under conditions characterized by insufficient lubrication, displacement can be derived from the equation. Consequently, the material's wear losses can be quantified using the following equation:

$$x(t) = e^{-\zeta\omega_n t}(C_1\cos\,\omega_d t\ + C_2\sin\omega_d t) + \frac{\frac{F_0}{K}\sin(\bar{\omega}t-\phi)}{\sqrt{(1-r^2)^2+(2r\zeta^2)^2}} \tag{27}$$

The vibration velocity, derived from the time derivative of displacement $x(t)$, is expressed by the following equation:

$$v(t) = e^{-\zeta\omega_n t}[-\zeta\omega_n t\ (C_1\cos(\omega_d t) + C_2\sin(\omega_d t)) - C_1\omega_d\sin(\omega_d t) + C_2\cos(\omega_d t)] + \frac{\frac{F_0}{k}\varpi\cos(\varpi t-\phi)}{\sqrt{(1-r^2)^2+(2r\zeta)^2}} \tag{28}$$

2.6 Sound Pressure. The energy emitted due to the frictional force between two surfaces can be quantified by measuring acoustic power. This parameter serves as a crucial element within the field of acoustics and is employed to evaluate the intensity of a sound source. The calculation of acoustic power P is conducted by applying the following equation [67,68]:

$$P = \rho_0 c S\sigma v^2 \tag{29}$$

where ρ_0 represents the density of air, c denotes the velocity of sound in air, S signifies cross-sectional area, σ indicates efficiency of radiation (which may be assumed to be equal to 1), and v, the vibrational velocity, can be determined using Eq. (29).

The sound power level L_w, which is characterized as a logarithmic metric that effectively measures the acoustic power radiated by a sound source, is determined by using the following equation:

$$L_w = 10\ \log_{10}\left(\frac{P}{P_r}\right) \tag{30}$$

where P_r is the reference power, which is quantified as 10–12 W.

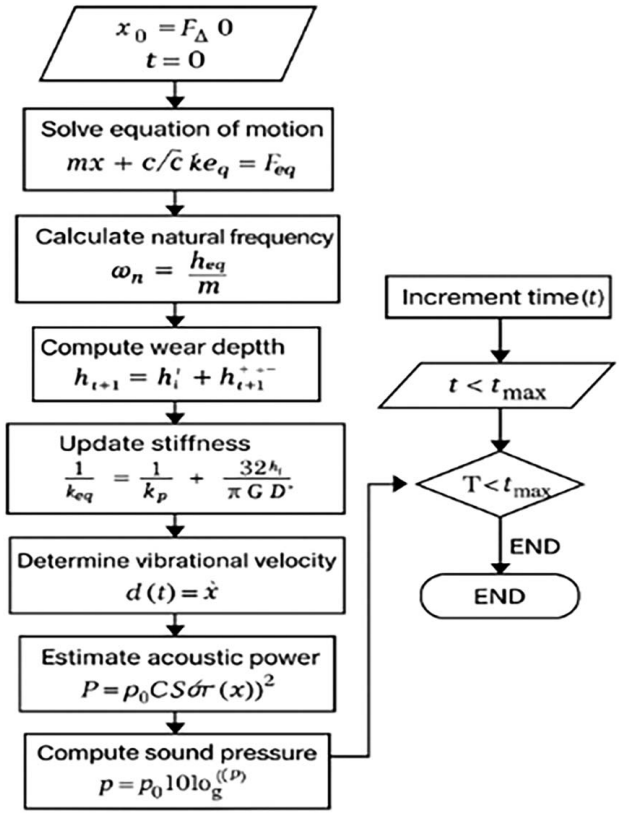

Fig. 5 The flowchart for the interdependence between mechanical wear, vibration response, and acoustic emission

The sound pressure level L_{p1}, which signifies the extent of auditory intensity perceived at a distance r from the source, is determined from the following equation:

$$L_{p1} = L_w + 10\ \log_{10}\left(\frac{Q}{4\pi r^2}\right) \tag{31}$$

where Q represents the directivity factor.

Upon the determination of the sound pressure level, the associated actual sound pressure quantified in pascals (Pa) can be derived in accordance with the following equation:

$$P = P_0 \times 10^{\frac{1}{20}L_{p1}} \tag{32}$$

where P_0 is the designated reference pressure quantified as 20×10^{-6} Pa.

Figure 5 illustrates the flowchart for the analytical model under lubrication conditions where the process is used to predict wear and sound in a pin-on-disc system. The model begins by setting the initial conditions, such as the pin's displacement due to elastic deformation, and setting the time to zero. The vibration equation is based on an SDOF system and incorporates the effects of mass, lubrication damping, and wear-induced stiffness changes. As the system runs, it continuously updates the stiffness by combining the fixed stiffness of the pin with the changing stiffness of the disc due to wear.

The system's natural frequency is determined by the current stiffness, and it fluctuates as wear increases and stiffness decreases. Archard's wear model and elastic deformation are used to calculate wear, which enables the model to capture both permanent wear and elastic changes at the contact. Using the pin's vibration velocity, the acoustic power can be calculated by assuming that sound travels freely in the air. This directly links the mechanical wear to the sound produced. The model transforms acoustic power into sound pressure levels, which are more readily measured in real-world systems.

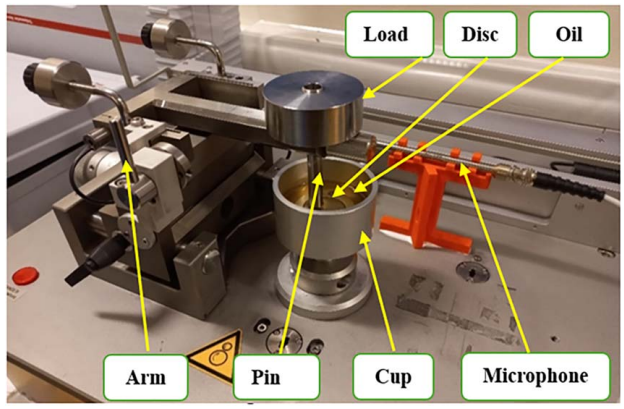

Fig. 6 The experimental pin-on-disc setup for wear depth and recording sound pressure under lubrication conditions

3 Experimental Scheme

An empirical investigation employing an Anton Paar TRB3 tribometer (Anton Paar, Graz, Austria) was executed within the manufacturing laboratory at Cranfield University, as illustrated in Fig. 6, and using a free-field microphone GRAS 40PP (with a sensitivity of 47.46 mV/Pa and a frequency response of 250 Hz) to record the frictional noise. The experimentation adhered to the requisite standards—ASTM G99, G133, and DIN 50324—thereby affirming that the TRB3 operates in full compliance with the principles of tribology [69,70]. The microphone is located at a constant distance of 10 cm from the center of the disc. The tribometer is equipped with a cantilever arm that enables the precise measurement of both the cumulative wear depth (penetration depth) and the relevant frictional parameters (coefficient of friction and frictional force). Table 1 shows that investigative trials were conducted using two different materials: mild steel and aluminum. The hardness was assessed in the laboratory under three different load conditions. The values for aluminum showed consistency, while the hardness of mild steel fluctuated with the increase of applied load. The procedures were executed with a sliding speed of 300 rpm and a radius of 10 mm. This analysis was performed under three loading conditions: 15 N, 20 N, and 30 N. The tests were conducted under

Table 1 The parameters and mechanical properties of materials

Pin stainless steel (440C)	
Diameter	6 mm
Radius	3 mm
Length	7.5 cm
Mass	39.872 g
Young's modulus	190 GPa
Poisson's ratio	0.27
Hardness	4414.5 MPa
Shear modulus (rigidity modulus)	82,000 MPa
Disc—aluminum	
Young's modulus	69 GPa
Poisson's ratio	0.33
Hardness under 15, 20, and 30 N	1103 MPa
Shear modulus (rigidity modulus)	27,000 MPa
Disc—mild steel	
Young's modulus	210 GPa
Poisson's ratio	0.3
Hardness under 15 N	2127 MPa
Hardness under 20 N	2236 MPa
Hardness under 30 N	2289 MPa
Shear modulus (rigidity modulus)	77,000 MPa

lubricated conditions using samples. The lubricant used had a viscosity of 30 W–50, and a total volume of 25 mL was assigned for all experimental trials. The duration allotted for each experiment was 180 s, with each test being repeated three times for greater accuracy. The laboratory environment's standard temperature was used for these experiments. The disc, with a diameter of 30 mm and a thickness of 5 mm, is securely affixed to the disc holder, while the stainless-steel pin has a diameter of 6 mm. The microphone can capture the emitted frictional noise, which is a form of sound pressure. By using an NI 9234 data acquisition card in an NI 9174 chassis, the microphone is connected to NI Signal Express, which enables in situ recordings at predetermined synchronized intervals.

The proposed analytical model, which is based on an SDOF system, was validated through the definition of experimental specifications. A variety of loads and materials were systematically varied to examine the model's efficacy across a wider spectrum of fluctuating parameters. During testing under lubrication conditions at reduced loads, the observed penetration depths are exceedingly minimal; hence, even slight augmentations in load can generate substantial discrepancies between the analytical forecasts and the empirical findings. Therefore, it is of utmost importance to validate the model under both high and low load conditions. Despite the operational constraints inherent in our experimental apparatus, we were unable to increase the load beyond 30 N without activating the safety threshold of the equipment. The disc materials employed in the experiments were mild steel and aluminum, as both materials are readily accessible in both academic and industrial environments for contact analysis and are extensively utilized in the manufacture of machine components. Furthermore, the chosen speed plays a significant role in the investigation of brake noise and wear characteristics.

4 Results and Discussion

Figure 7 presents the comparison between analytical and experimental wear depth measurements over time for aluminum and mild steel under loads of 15 N, 20 N, and 30 N. For all test conditions, wear depth increases with time and applied load, as expected. The experimental trends are closely followed by the analytical model, particularly at medium and high loads. The low magnitudes of wear are the reason for the small deviations observed at lower loads. Figure 8 compares analytical and experimental sound pressure values. The results confirm that the emitted sound pressure increases with load and test duration due to increased frictional interaction and material removal. The analytical predictions again align well with the measured values for both the rate of increase and overall magnitude of sound pressure under all load conditions.

To quantify model accuracy, Fig. 9 shows the percentage errors between analytical predictions and experimental results for both final wear depth and sound pressure. The errors for wear depth are between 10.0% and 31.7%. At lower loads (AL15N and AL20N), aluminum displays the greatest discrepancies, probably due to its softer material properties and greater sensitivity to microstructural variations. Mild steel displays better agreement, with errors remaining below 22%, especially when under higher loads. The figure demonstrates the percentage error in sound pressure predictions, which varies from 13.7% to 21.1%. The inherent complexity of acoustic measurements makes it acceptable for these deviations to be accepted. At higher loads, the model tends to underestimate the sound pressure for aluminum and overestimate it for mild steel. Despite these variations, the consistent trends between predicted and measured values validate the reliability of the analytical model in capturing the wear–friction–noise relationship under lubricated conditions.

Figure 10 demonstrates the wear depth over time at each load. The analytical predictions for aluminum indicate a slight increase in wear rates compared to those measured at 15 N, but the predicted and measured values tend to align more as the load increases. This may be attributed to aluminum's softer surface and its greater tendency toward plastic deformation and adhesion under increased load. For mild steel, the model closely follows the experimental data for all loads. The emitted sound pressure for both materials increased with time at each load, as shown in Fig. 11. It is observed that aluminum consistently produces a higher sound pressure than mild steel at equivalent loads, which is due to its higher friction and wear rate under the same sliding conditions.

To further validate the model and evaluate material-specific behavior, wear and sound pressure results were separated by material. Figure 12 presents a comparison between analytical and experimental results for wear depth and sound pressure over time for mild steel under loads of 15 N, 20 N, and 30 N. In all cases, both analytical

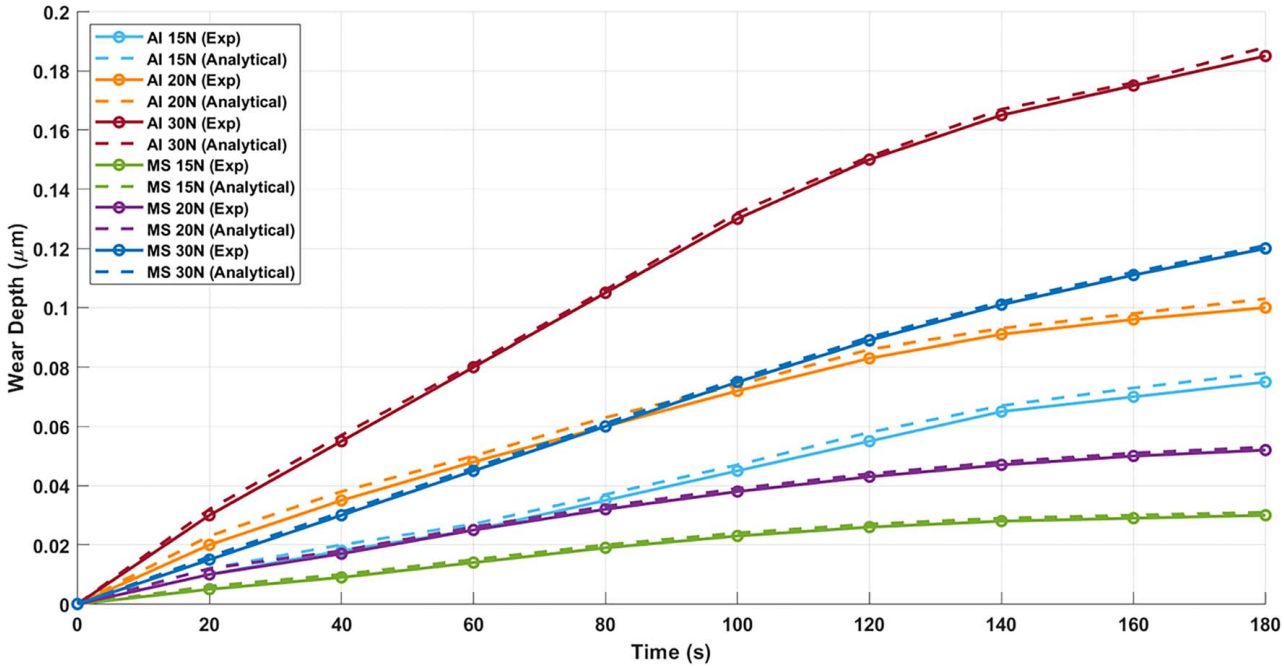

Fig. 7 Comparison between analytical and experimental wear depth with time under lubricated conditions

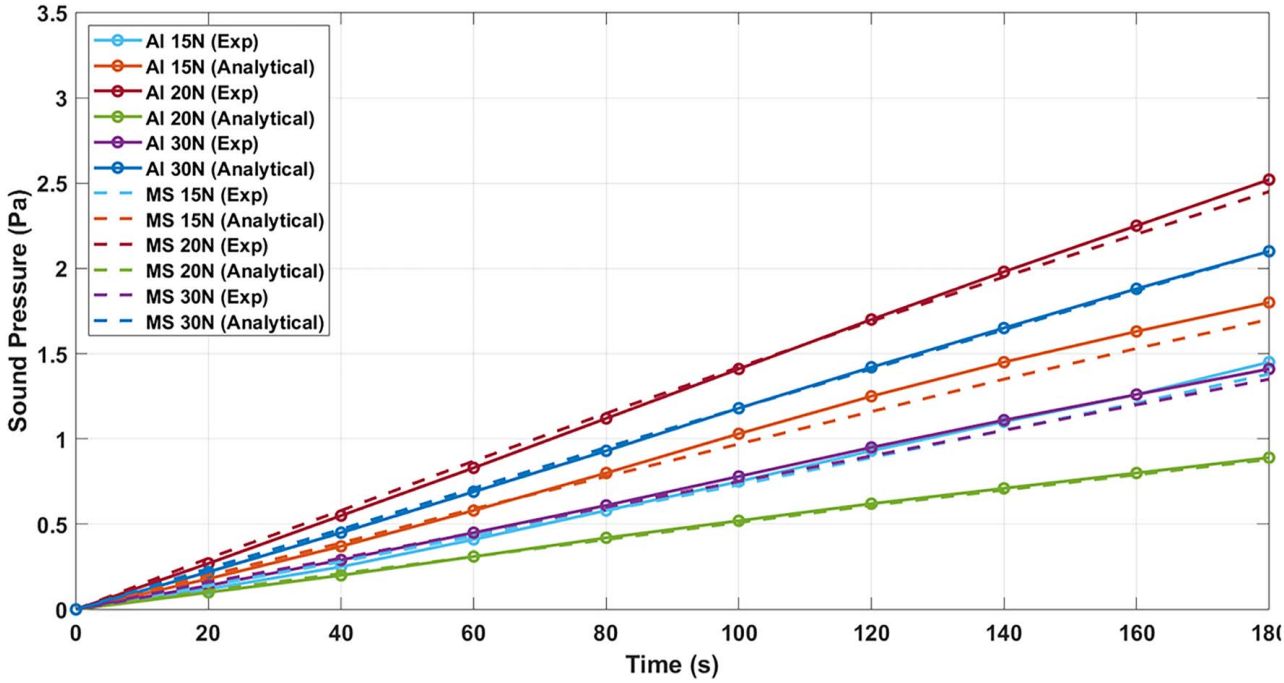

Fig. 8 Comparison between analytical and experimental cumulative sound pressure with time under lubricated conditions

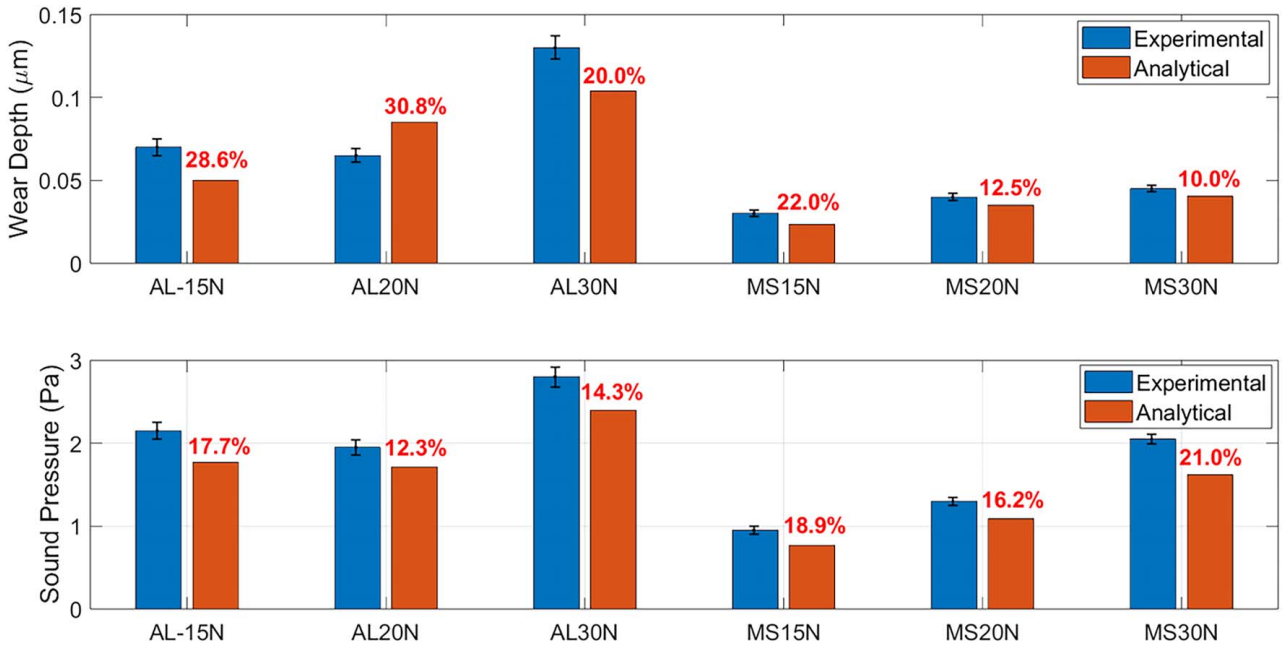

Fig. 9 The percentage errors for analytical and empirical results for cumulative wear depth and acoustic pressure

and experimental wear depth curves exhibit a monotonic increase, consistent with steady-state wear under lubricated sliding conditions. The agreement is firm at 15 N and 20 N, where the wearer remains below 0.06 μm, confirming the model's accuracy in low-to-moderate load ranges. The wear depth increases to about 0.12 μm at 30 N, with a slight difference between experimental and analytical values, probably due to micro-plastic deformation effects. Correspondingly, sound pressure also rises with load and time; the close agreement between values for both analytical predictions and measured values confirms a strong correlation between sound pressure and wear depth. Noise generating mechanisms that are more complex, such as asperity fracture or lubricant instability, are responsible for minor deviations at higher loads. Figure 13 compares aluminum similarly when using the same load range. The wear depth is almost linear, and both calculations and experiments are consistent at every load level. The wear is low at 15 N, but it increases at 20 N and becomes higher at 30 N, which is in line with the predicted trends. The wear values of aluminum are slightly higher than those of mild steel because of its softer nature. The analytical predictions are closely matched to the experimental results, with only minor discrepancies observed at the highest load, possibly due to thermal effects or localized softening

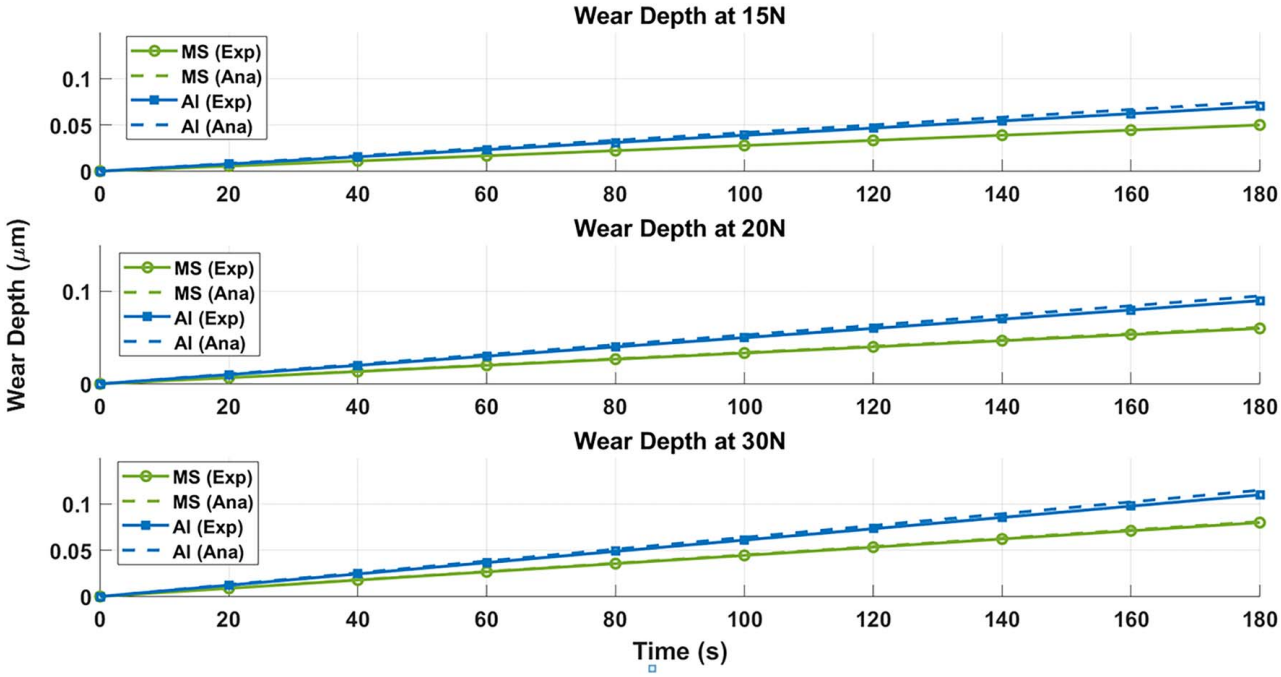

Fig. 10 Comparison between analytical and experimental wear depth under different loads

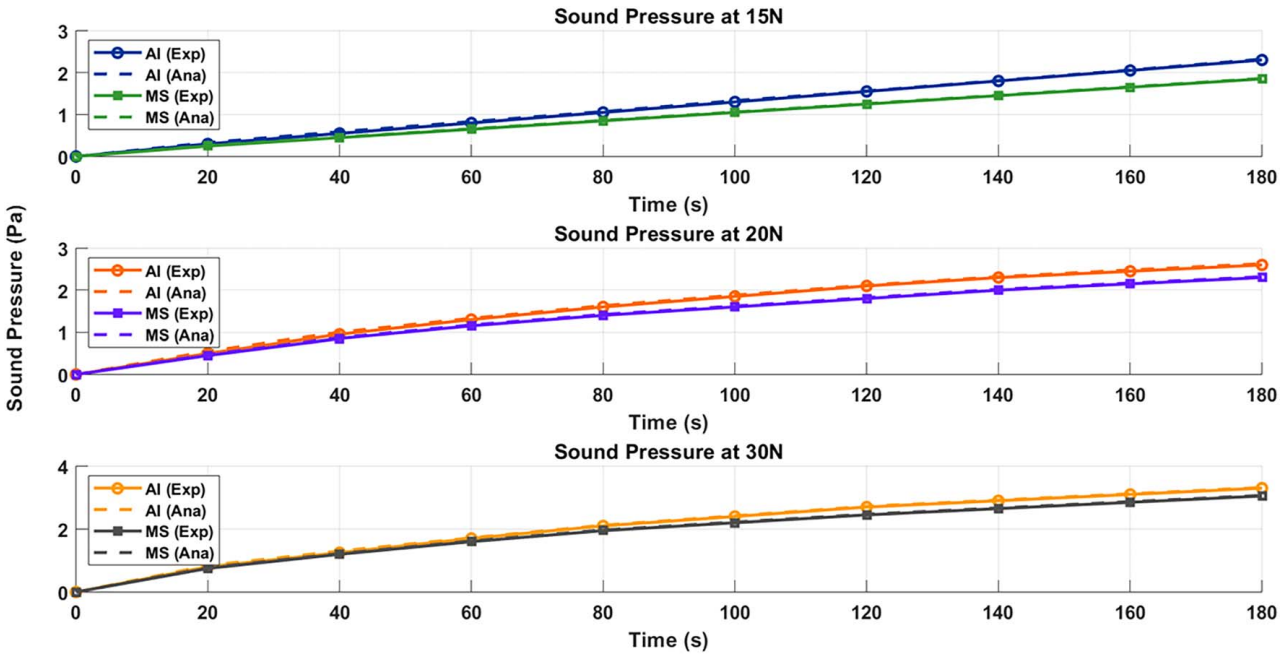

Fig. 11 Comparison between analytical and empirical total sound pressure as a function of time

that are not considered in the model. The measured sound pressure results follow the same load-dependent trend, increasing from 1.5 Pa at 15 N to nearly 3.5 Pa at 30 N. The analytical values align closely with the experimental data, demonstrating the model's ability to simulate both wear and friction-induced noise in softer materials.

Furthermore, a comparison was made with Basit et al. [60], a model that predicts wear and frictional noise in dry contact conditions. Our model's accuracy in lubricated scenarios is demonstrated by its ability to predict both wear depth and sound pressure. At a load of 30 N, our model has a wear depth error of 10.0%, whereas the dry contact model is 25.9%. Similarly, the sound pressure error remains within 21.1% in our case, versus 14.4% reported by Basit et al. This indicates that the proposed vibration-based approach is not only consistent with previously published models but also better adapted to real-world lubricated conditions.

The results across both materials and the three loads validate the effectiveness of the proposed model in providing a reliable approximation of both tribological and acoustic behavior under lubricated conditions. Mild steel, due to its greater hardness, exhibited lower wear and sound pressure values compared to aluminum under identical loading conditions as predicted by the model.

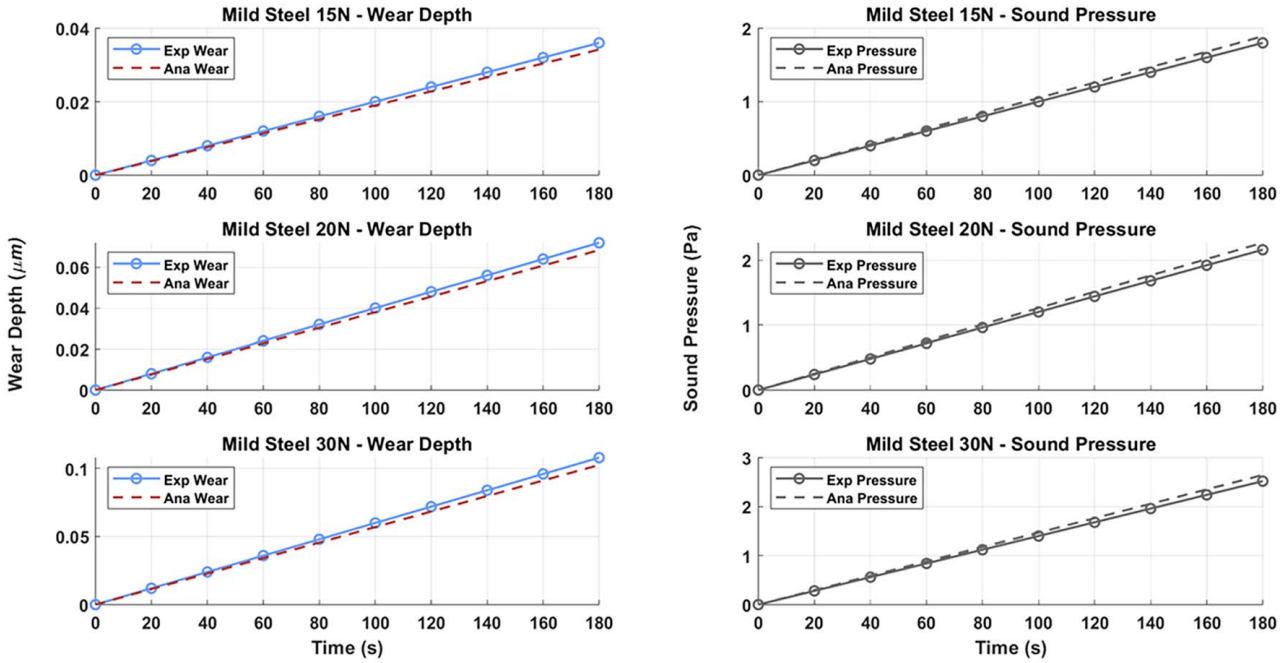

Fig. 12 Comparison of analytical predictions and experimental wear depths for mild steel under different loads

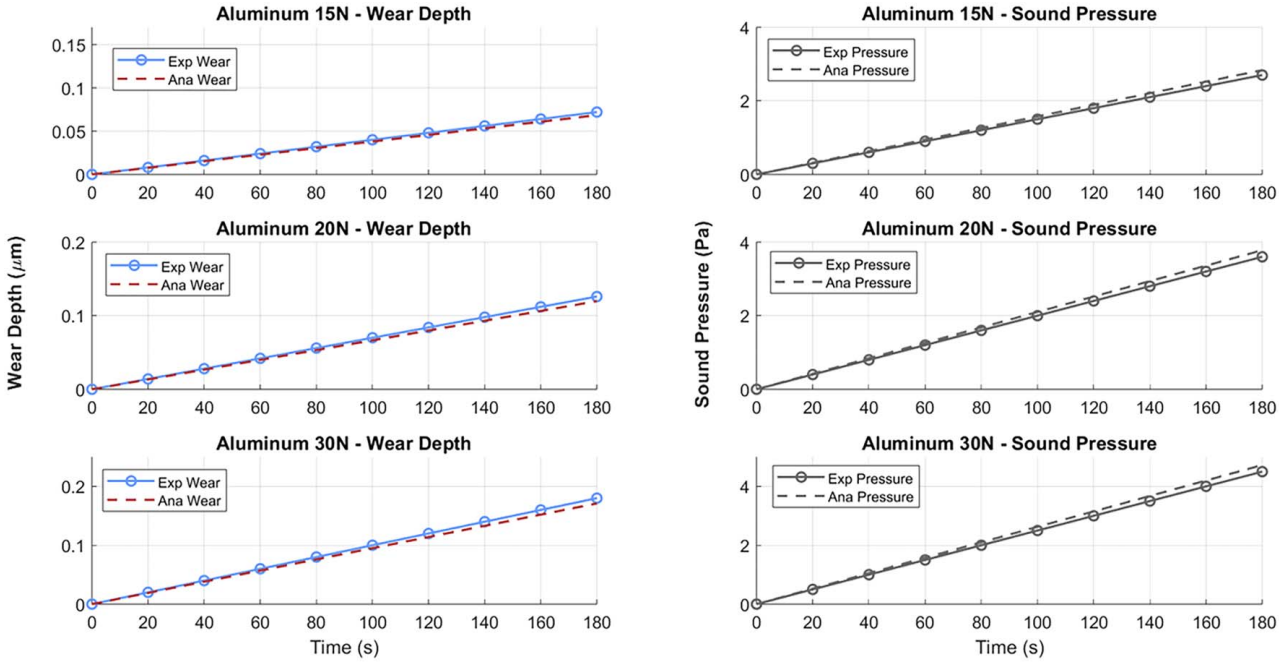

Fig. 13 Comparison of analytical predictions and experimental wear depths for aluminum under different loads

5 Analysis of Scar Profile and Depth Under Both Dry and Lubricated Conditions

To further validate the experimental wear results, additional tests were performed under dry sliding conditions with the same parameters. Direct comparison of penetration depth between dry and lubricated scenarios was made possible. The wear scar profiles were measured using a Taylor Hobson surface profilometer, as shown in Fig. 14, while the wear scars themselves were visually examined using a Zeiss Axio Zoom V16 digital microscope. The tribological characteristics exhibited by mild steel subjected to a load and conditions, subjected to a 30-N load, were systematically examined and analyzed using wear depth profiles along the radial axis of the disc surface (ranging from 0 to 10 mm). Both dry and lubricated sliding conditions were used to thoroughly test each material. However, for mild steel at 20 N under a lubrication condition, the wear profile remained stable and shallow across the radial span, indicating minimal material removal. The effective reduction of friction and surface protection provided by lubrication is reflected in this stability. The lower panels present results for dry and lubricated wear profiles for aluminum at 30 N. Under dry conditions, the wear scar exhibits a pronounced depth exceeding 100 μm,

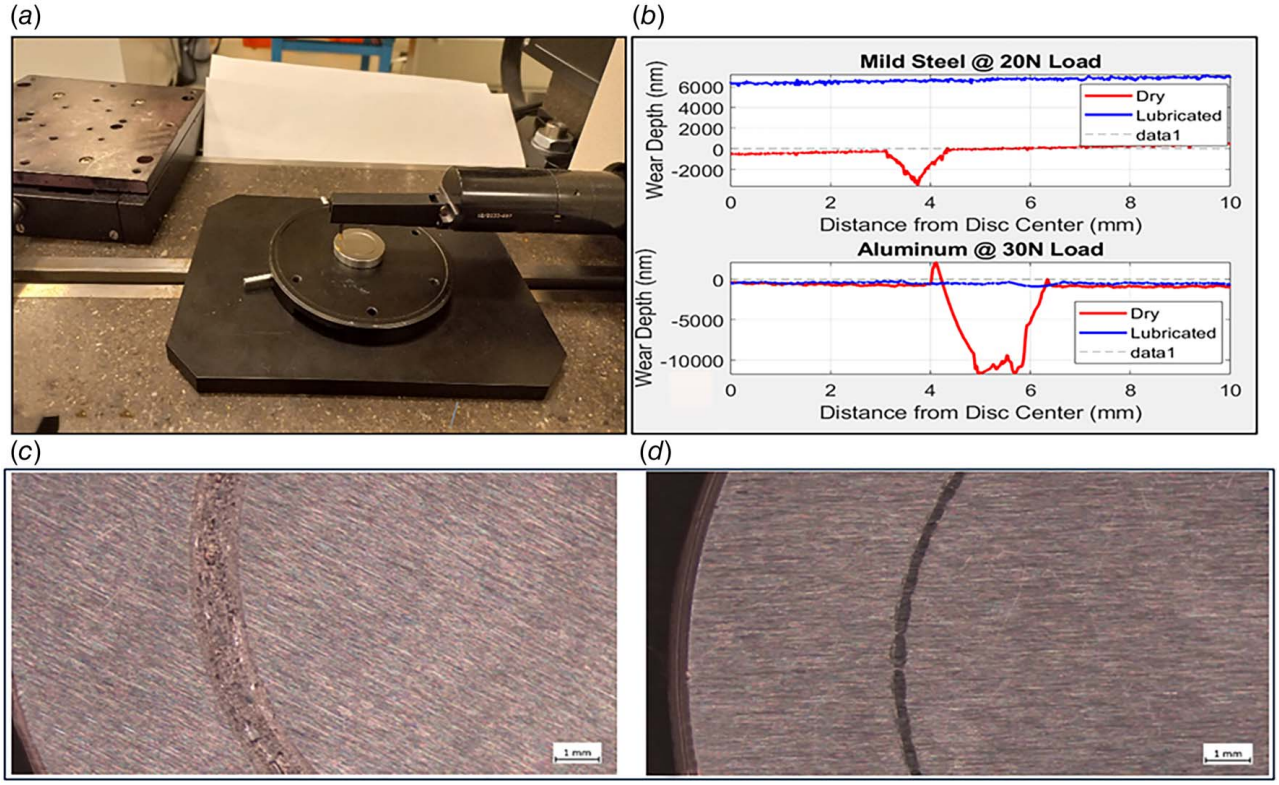

Fig. 14 For additional validation, the Taylor Hobson surface profilometer tester was employed. Figures (*a*) and (*b*) present the material tested under dry (solid line) and lubricated (dashed line) conditions, while fig. (*c*) illustrates the wear track of mild steel under dry conditions and fig. (*d*) shows the wear track under lubrication conditions.

suggesting severe material loss likely due to adhesive wear and high friction. However, the lubricated profile is markedly smoother and shallower, with minimal surface penetration. This highlights the significant role of lubrication in reducing wear, particularly in softer materials under higher loads. These findings demonstrate the effectiveness of lubrication in mitigating wear in both materials, with a more pronounced impact observed for aluminum due to its lower hardness value and higher susceptibility to adhesive wear. Figure 14(*b*) shows wear scar profiles under dry and lubricated conditions, with (*b*) wear depth profiles obtained using Taylor Hobson surface profilometry and corresponding wear scar images.

A Zeiss Axio Zoom V16 digital microscope was used for microscopic analysis to gain more insight into the wear mechanisms. With dry mild steel subject to a load of 30 N, as shown in Figs. 14(*c*) and 14(*d*), the wear track on the dry-tested mild steel appears rough and irregular, characterized by deep scratches, loose debris, and signs of material detachment. The surface has unevenness and becomes dark, which indicates intense wear and tear. Profilometry results confirmed significant material loss because the worn region is vast and distinct from the unworn areas. When lubricated mild steel is subjected to a 30 N load, the wear track becomes significantly smoother and narrower. There is a reduction in the amount of wear debris observed, and the surface appears cleaner and more uniform. This implies that lubrication effectively reduces friction and protects the surface, resulting in milder wear. Compared to the dry case, the depth and severity of wear are significantly reduced.

In summary, the results confirm that wear depth and sound pressure both increase with applied load and test duration and that the analytical predictions generally align well with the experimental data for both mild steel and aluminum. The softer aluminum experiences minor deviations at lower loads, likely because of microstructural factors and plastic deformation effects. Despite this, the model is still accurate enough for wear-life forecasting and noise-based condition monitoring. During the initial lubrication tests, relatively small friction and wear values were observed, as the applied loads of 5 N and testing duration were both relatively low, limiting the extent of measurable wear and frictional effects. To obtain more pronounced data for improved analysis, the loads were incrementally increased to 30 N, and the test duration was extended. The larger, more discernible wear tracks were a result of these adjustments, which enabled a deeper understanding of material performance under lubricated conditions. Additionally, parallel tests under dry conditions revealed significantly higher wear rates, particularly for aluminum, underscoring the protective role of lubrication in reducing friction and material removal. In general, the proposed model's predictions were closely aligned with experimental findings, providing valuable insights into the comparison of dry and lubricated wear tracks.

The model could be validated under more extreme conditions by extending the experimental range, even though the current study focused on loads up to 30 N. The model's accuracy could be improved by incorporating temperature-dependent effects and surface roughness evolution, as these factors can have a significant impact on lubrication properties and wear mechanisms. The integration of finite element modeling in future studies will enable the simulation of detailed contact mechanics and stress distributions under both dry and lubricated conditions. The model's accuracy and practical relevance will be enhanced by a comprehensive comparison between analytical, experimental, and numerical results.

6 Conclusions

This study presented a novel analytical model that unifies friction, wear, and noise under lubricated conditions by combining SDOF vibration theory, Hertz contact mechanics, Archard's wear model, and acoustic emission principles. A thin lubricating film's viscous damping effects are dynamically integrated into the

model, allowing real-time updates to contact stiffness and wear depth. The proposed model's ability to accurately capture both wear depth and sound pressure trends was demonstrated through validation experiments on mild steel and aluminum discs at three loads. The accuracy of wear depth predictions was generally below 31%, which indicates good reliability for both aluminum (softer material) and mild steel. Sound pressure levels deviated by approximately 14–21% of the recorded data, which is acceptable given the inherent variability in acoustic emissions and lubrication film behavior, where the incorporated lubrication acts as a damping mechanism. The model reproduced experimental observations more accurately than comparable dry-condition models [60]. Thin-film dynamics capture in tribological analyses is crucial due to the significant impact of lubrication on both friction-induced vibrations and noise. The developed integrated friction–wear–noise model offers a robust tool for real-time tribological monitoring, aligning with industrial needs for predictive maintenance and reduced downtime. Its ability to accommodate various materials across a wide range of loads and speeds enhances its versatility, making it suitable for diverse mechanical systems such as gearboxes, brake assemblies, and rotating machinery.

Conflict of Interest

There are no conflicts of interest.

Data Availability Statement

The datasets generated and supporting the findings of this article are obtainable from the corresponding author upon reasonable request.

Nomenclature

Abbreviations

AE = Acoustic emission
SDOF = single-degree freedom
TRB3 = Tribometer tester

References

[1] Pawlik, P., 2023, "The Acoustic Method for Diagnosing Machines Operating Under Variable Conditions," Inst. Noise Control Eng., **23**, pp. 5878–5883.
[2] Jombo, G., and Zhang, Y., 2023, "Acoustic-Based Machine Condition Monitoring—Methods and Challenges," Engineering, **4**(1), pp. 47–79.
[3] Kalifa, M., Starr, A., and Khan, M., 2025, "Current Research and Challenges in Modeling Wear, Friction, and Noise in Mechanical Contacts," Proc. Inst. Mech. Eng., Part J: J. Eng. Tribol., **1**(21), pp. 985–1005.
[4] Rastegaev, I., Merson, D., Rastegaeva, I., and Vinogradov, A., 2020, "A Time-Frequency Based Approach for Acoustic Emission Assessment of Sliding Wear," Lubricants, **8**(52), pp. 4–11.
[5] Rahman, A., Khan, M., and Mushtaq, A., 2021, "Predictive Modeling of Surface Wear in Mechanical Contacts Under Lubricated and Non-Lubricated Conditions," Sensors, **21**(4), pp. 1–16.
[6] Yonemura, S., Zhou, L., and Talke, F. E., 2003, "An Investigation of Slider Vibrations in Near Contact Recording Using a Digital Laser Doppler Vibrometer," ASME J. Tribol., **125**(3), pp. 571–575.
[7] Fan, Y., Gu, F., and Ball, A., 2010, "Modeling Acoustic Emissions Generated by Sliding Friction," Wear, **268**(5–6), pp. 811–815.
[8] Doğanay Katı, H., Buhari, J., Francese, A., He, F., and Khan, M., 2025, "Numerical Analysis of Crack Path Effects on the Vibration Behavior of Aluminum Alloy Beams and Its Identification via Artificial Neural Networks," Intell. Sens., **25**(3), pp. 2–10.
[9] Baccar, D., Schiffer, S., Söffker, D., and Cam, L., 2014, "Acoustic Emission-Based Identification and Classification of Frictional Wear of Metallic Surfaces," Seventh European Workshop on Structural Health Monitoring, Nantes, France, July 8–11, pp. 1178–1185.
[10] Feng, P., Borghesani, P., Smith, W. A., Randall, R. B., and Peng, Z., 2020, "A Review on the Relationships Between Acoustic Emission, Friction and Wear in Mechanical Systems," Appl. Mech. Rev., **72**(2), pp. 1–17.
[11] Rathee, R., 2023, "Numerical Modeling and Simulation of Friction Models for Mechanical Systems: A Brief Review," Mater. Today Proc., **12**(1), pp. 4–12.
[12] Lontin, K., and Khan, M., 2021, "Interdependence of Friction, Wear, and Noise: A Review," Friction, **9**(6), pp. 1319–1345.
[13] Kalifa, M., Starr, A., and Khan, M., 2023, "Limitations in the Existing Models for Predicting Accurate Interdependencies Between Wear and Friction Noise," 19th Int. Conf. Cond. Monit. Asset Manage., **12**(11), pp. 1–12.
[14] Alberto, F., Weiffenbach, L., and Romero, F., 2024, "Experimental Analysis of Acoustic Emissions in Rolling and Sliding Friction: Implications to Gear Transmissions," Res. Sq, **1**(3), pp. 1–18.
[15] Scheeren, B., Thakoerdajal, N., and Pahlavan, L., 2024, "Influence of Grease Contamination on Acoustic Emission Monitoring of Low-Speed Roller Bearings," 11th European Workshop on Structural Health Monitoring, Potsdam, Germany, June 10–13, pp. 1–8.
[16] Bote-Garcia, J.-L., Mokhtari, N., and Gühmann, C., 2020, "Wear Monitoring of Journal Bearings With Acoustic Emission Under Different Operating Conditions," PHM Soc. Eur. Conf., **5**(1), p. 8.
[17] Chen, J., Lu, J., Hou, Y., Ding, X., and Zhang, W., 2024, "Study on the Friction Behavior and Abnormal Conditions of Non-Contact Mechanical Seal Based on Acoustic Emission," Tribol. Lett., **72**(3).
[18] Akay, A., 2002, "Acoustics of Friction," J. Acoust. Soc. Am., **111**(4), pp. 1525–1548.
[19] Stoimenov, B. L., Maruyama, S., Adachi, K., and Kato, K., 2007, "The Roughness Effect on the Frequency of Frictional Sound," Tribol. Int., **40**(4), pp. 659–664.
[20] Ben Abdelounis, H., Zahouani, H., Le Bot, A., Perret-Liaudet, A., Tkaya, J., and Tkaya, M. B., 2011, "Numerical Simulation of Friction Noise," Wear, **271**(3–4), pp. 621–624.
[21] Yokoi, M., and Nakai, M., 1976, "A Fundamental Study on Frictional Noise," JSME, **22**(173), pp. 1665–1671.
[22] Wang, X. C., Mo, J. L., Ouyang, H., Wang, D. W., Chen, G. X., Zhu, M. H., and Zhou, Z. R., 2016, "Squeal Noise of Friction Material With Groove-Textured Surface: An Experimental and Numerical Analysis," ASME J. Tribol., **138**(2), pp. 15–1098.
[23] Towsyfyan, H., Gu, F., Ball, A. D., and Liang, B., 2018, "Modeling Acoustic Emissions Generated by Tribological Behavior of Mechanical Seals for Condition Monitoring and Fault Detection," Tribol. Int., **125**, pp. 46–58.
[24] Othman, M. O., and Elkholy, A. H., 1990, "Surface-Roughness Measurement Using Dry Friction Noise," Exp. Mech., **30**(3), pp. 309–312.
[25] Shahid, M. A., M, Khan, T. M., T, Lontin, K., K, Basit, K., K, and Khan, M., M, 2020, "Multiple Point Contact Wear Prediction and Source Identification Scheme Using a Single Channel Blended Airborne Acoustic Signature," IFAC-Papers Online, **53**(3), pp. 283–288.
[26] Chen, S., Cheng, G., Guo, F., Jia, X., and Wen, X., 2025, "Integrating Friction Noise for In Situ Monitoring of Polymer Wear Performance: A Machine Learning Approach in Tribology," ASME J. Tribol., **147**(6), p. 061701.
[27] Wang, M., 2025, "Transfer Models and Standard Models for Predicting Wear-Rates on the Basis of Friction Noise: A Comparative Study," ASME J. Tribol., **147**(6), p. 061702.
[28] Raja, J. E., Kiong, L. C., and Soong, L. W., 2013, "Hilbert-Huang Transform-Based Emitted Sound Signal Analysis for Tool Flank Wear Monitoring." https://link.springer.com/article/10.1007/s13369-013-0580-7.
[29] Khan, M. A., Basit, K., Khan, S. Z., Khan, K. A., and Starr, A. G., 2017, "Experimental Assessment of Multiple Contact Wear Using Airborne Noise Under Dry and Lubricated Conditions," Part J: J. Eng. Tribol., **231**(12), pp. 1503–1516.
[30] Tian, Y., Kalifa, M., Khan, M., and Yang, Y., 2024, "Interplay Between Wear and Thermal Expansion in 6082 Aluminum: A Simulation and Experimental Study," Appl. Sci., **14**(23), pp. 1–18.
[31] Lontin, K., Khan, M., and Alharbi, B., 2022, "Investigation of the Effect of Temperature on the Wear Rate and Airborne Noise in Sliding Wear," Materials, **15**(3), p. 812.
[32] Hase, A., Mishina, H., and Wada, M., 2016, "Fundamental Study on Early Detection of Seizure in Journal Bearing by Using Acoustic Emission Technique," Wear, **346–347**(347), pp. 132–139.
[33] Hase, A., Mishina, H., and Wada, M., 2012, "Correlation Between Features of Acoustic Emission Signals and Mechanical Wear Mechanisms," Wear, **292–293**, pp. 144–150.
[34] Elasha, F., Greaves, M., Mba, D., and Fang, D., 2017, "A Comparative Study of the Effectiveness of Vibration and Acoustic Emission in Diagnosing a Defective Bearing in a Planetry Gearbox," Appl. Acoust., **115**, pp. 181–195.
[35] Albers, A., Burger, W., Sovino, R., and Dickerhof, M., 2006, "Monitoring Lubrication Regimes in Sliding Bearings—Using Acoustic Emission Analysis," Pract. Oil Anal., **8**(5), pp. 10–13. http://digbib.ubka.uni-karlsruhe.de/volltexte/1000007083.
[36] Albers, A., and Dickerhof, M., 2016, "Simultaneous Monitoring of Rolling-Element and Journal Bearings Using Analysis of Structure-Born Ultrasound Acoustic Emissions," Int. Mech. Eng. Congr. Expos., **12**(18), pp. 1–9.
[37] Mokhtari, N., Pelham, J. G., Nowoisky, S., Bote-Garcia, J. L., and Gühmann, C., 2020, "Friction and Wear Monitoring Methods for Journal Bearings of Geared Turbofans Based on Acoustic Emission Signals and Machine Learning," Lubricants, **8**(3), pp. 1–27.
[38] Zhang, H., Wang, W., Zhang, S., and Zhao, Z., 2017, "Modeling of Elastic Finite-Length Space Rolling-Sliding Contact Problem," Tribol. Int., **113**(July 2016), pp. 224–237.
[39] Zhang, Z., Yin, N., Chen, S., and Liu, C., 2021, "Tribo-Informatics: Concept, Architecture, and Case Study," Friction, **9**(3), pp. 642–655.
[40] Ferrando Chacon, J. L., Artigao Andicoberry, E., Kappatos, V., Asfis, G., Gan, T. H., and Balachandran, W., 2014, "Shaft Angular Misalignment Detection Using Acoustic Emission," Appl. Acoust., **85**, pp. 12–22.

[41] Xiang, Z. Y., Mo, J. L., Ouyang, H., Massi, F., Tang, B., and Zhou, Z. R., 2020, "Contact Behavior and Vibrational Response of a High-Speed Train Brake Friction Block," Tribol. Int., **152**, p. 106540.
[42] Wang, H., Liu, Z., Zou, L., and Yang, J., 2017, "Influence of Both Friction and Wear on the Vibration of Marine Water Lubricated Rubber Bearing," Wear, **376–377**, pp. 920–930.
[43] Le Bot, A., 2017, "Noise of Sliding Rough Contact," J. Phys.: Conf. Ser, **21**(4), pp. 2–6.
[44] Seong, Y., Lee, D., Yeom, J., and Park, J., 2021, "The Feature Extraction Through Wavelet Coefficients of Metal Friction Noise for Adhesive and Abrasive Wear Monitoring," Appl. Sci., **11**(9), pp. 1–10.
[45] Albuquerque de Freitas, T. V., Nascimento Rodrigues, R. d., Santos Costa, C. A., Araujo Bezerra, R. d., Vieira Gonçalves, V., and Cardoso Maciel, M. H., 2024, "Parametric Analysis of the Relationship Between Squeal and Friction Wear in Motorcycle Disc Brakes," Part J: J. Eng. Tribol., **238**(11), pp. 1433–1448.
[46] Ma, B., Lu, W., Yu, L., Xiong, C., D, G., and C, X., 2024, "Friction-Wear and Noise Characteristics of Friction Disks With Circular Texture," Materials, **17**(23), pp. 1–12.
[47] Wang, Y., Zhang, Y., and Long, R., 2023, "Influence of Pits on the Tribological Properties and Friction-Induced Vibration Noise of Textured Tapered Roller Bearings," Tribol. Trans., **66**(3), pp. 399–412.
[48] Zhang, D., Li, Z., Zhao, F., Gao, F., Gao, Z., Zhang, H., and Dong, G., 2021, "Study on Tribological Behavior of Grooved-Texture Surfaces Under Sand–Oil Boundary Lubrication Conditions," Tribol. Trans., **64**(1), pp. 167–177.
[49] Liu, S., Sai, Q., Wang, S., and Williams, J., 2022, "Effects of Laser Surface Texturing and Lubrication on the Vibrational and Tribological Performance of Sliding Contact," Lubricants, **10**(1), pp. 2–8.
[50] Boness, R. J., Mcbride, S. L., and Sobczyk, M., 1990, "Wear Studies Using Acoustic Emission Techniques," Tribol. Int., **23**(5), pp. 291–295.
[51] Ta, T. N., Horng, J. H., and Hwang, Y. L., 2022, "Correlation Between Tribological and Vibration Behaviors in Sliding Lubricated Contacts," ASME J. Tribol., **144**(11), p. 111603.
[52] Xing, P., Zhu, Y., Li, G., Liu, T., Gao, H., Song, Y., and Zhang, H., 2023, "A Detecting Method for 'Weak' Friction-Induced Vibration Based on Cross-Correlation Analysis Between Vibration and Sound Signals," Appl. Sci., **13**(13), pp. 4–11.
[53] Benabdallah, H. S., and Aguilar, D. A., 2008, "Acoustic Emission and Its Relationship With Friction and Wear for Sliding Contact," Tribol. Trans., **51**(6), pp. 738–747.
[54] De Moerlooze, K., Al-Bender, F., and Van Brussel, H., 2010, "A Generalised Asperity-Based Friction Model," Tribol. Lett., **40**(1), pp. 113–130.
[55] Eriten, M., Polycarpou, A. A., and Bergman, L. A., 2012, "A Physics-Based Friction Model and Integration to a Simple Dynamical System," ASME J. Vib. Acoust., **134**(5), p. 051012.
[56] Emami, A., Khaleghian, S., Su, C., and Taheri, S., 2017, "Physics-Based Friction Model With Potential Application in Numerical Models for Tire-Road Traction," Dyn. Syst. Control Conf., DSCC, **3**, pp. 1–6.
[57] Liu, T., Liu, G., Xie, Q., and Wang, Q. J., 2006, "Two-Dimensional Adaptive-Surface Elasto-Plastic Asperity Contact Model," ASME J. Tribol., **128**(4), pp. 898–903.
[58] Tian, Y., Khan, M., Deng, H., and Omar, I., 2025, "Quantifying the Interrelationship Between Friction, Wear, and Noise: A Comparative Study on Aluminum, Brass, and Steel," Tribol. Int., **203**(September 2024), p. 110403.
[59] Lontin, K., and Khan, M. A., 2021, "Wear and Airborne Noise Interdependency at Asperitical Level: Analytical Modeling and Experimental Validation," Materials, **14**(23), p. 7308.
[60] Basit, K., Shams, H., Khan, M. A., and Mansoor, A., 2023, "Vibration Analysis Approach to Model Incremental Wear and Associated Sound in Multi-Contact Sliding Friction Mechanisms," ASME J. Tribol., **145**(9), p. 091109.
[61] Moon Kyu, K., 2021, *Dynamic Modeling and Active Vibration Control of Structures*, Springer.
[62] Rao, S. S., 2004, "Mechanical Vibrations." https://www.researchgate.net/profile/V-TNguyen/publication/273330566_Basic_Mechanical_Vibrations/links/54fecf170cf2741b69f164f2/Basic-Mechanical-Vibrations.pdf.
[63] Timoshenko, S., and Goodier, J, 2005, *Theory of Elasticity*, 3rd ed., Vol. 3, Spring, New York.
[64] Archard, J. F., 1953, "Contact and Rubbing of Flat Surfaces," J. Appl. Phys., **24**(8), pp. 981–988.
[65] Johnson, K. L., 1982, "One Hundred Years of Hertz Contact," Proc. Inst. Mech. Eng., **196**(1), pp. 363–378.
[66] Hegadekatte, V., Huber, N., and Kraft, O., 2006, "Modeling and Simulation of Wear in a Pin on Disc Tribometer," Tribol. Lett., **24**(1), pp. 51–60.
[67] Hofler, T., 1988, "Accurate Acoustic Power Measurements With a High-Intensity Driver," J. Acoust. Soc. Am., **83**(2), pp. 777–786.
[68] Tao, C., Guo, G., Ma, Q., Tu, J., Zhang, D., and Hu, J., 2017, "Accurate Acoustic Power Measurement for Low-Intensity Focused Ultrasound Using Focal Axial Vibration Velocity," J. Appl. Phys., **122**(1), pp. 4–9.
[69] ASTM D 3576, 2018, "Standard Test Method for Linearly Reciprocating Ball-on-Flat Sliding Wear G133-22," Designation: E 778–87, **i**, pp. 3–5. https://pdfcoffee.com/wear-testing-with-a-pin-on-disk-apparatus-standard-test-method-for-pdf-free.html.
[70] Conshohocken, W., 2007, "Standard Test Method for Wear Testing With a Pin-on-Disk Apparatus G99-95a," Wear, **v**, pp. 1–5. https://store.astm.org/g0099-17.html.

Analytical modeling and experimental validation of wear and frictional noise under lubricated conditions

Kalifa, Mohamed

2026-01-01

Kalifa M, Khan M, He F, et al., (2026) Analytical modeling and experimental validation of wear and frictional noise under lubricated conditions. Journal of Tribology, Volume 148, January 2026, Article number 011706

https://doi.org/10.1115/1.4069335